Supplementary Information

Tables, Figures, and Movies

Concentration condition	Nanodrop (mg/ml)	Concentrating efficiency (Nanodrop)	Volume (µl)	Concentrating efficiency (volume)	Alexa Fluor 594 dextran intensity	Concentrating efficiency (dextran dye)	Oscillation or not
Vacuum evap, 0 min 1x 50 µl	206.99	1.00	50	1.00	3081.61±124.64	1.00	Yes
Vacuum evap, 10 min 2x 40 µl	228.48	1.10	~70	1.14	3301.04±127.16	1.08	Yes
Vacuum evap, 20 min 2x 40 µl	244.44	1.18	~60	1.27	3543.35±137.28	1.16	Yes
Vacuum evap, 30 min 3x 40 µl	268.97	1.30	~85	1.42	3708.52±543.43	1.22	Yes
Vacuum evap, 40 min 3x 40 µl	299.76	1.45	miss	miss	4370.06±236.22	1.46	No
Mix extract buffer with 40-min extract	--	--	--	--	--	--	Yes

Table S1: Three methods are applied to calculate the concentrating efficiency of vacuum evaporation. Dextran intensity of each condition is quantified from fitting the histogram of droplet intensity to a normal distribution. By comparing these three methods, we choose fluorescence intensity changes before and after evaporation as the primary method for quantification.

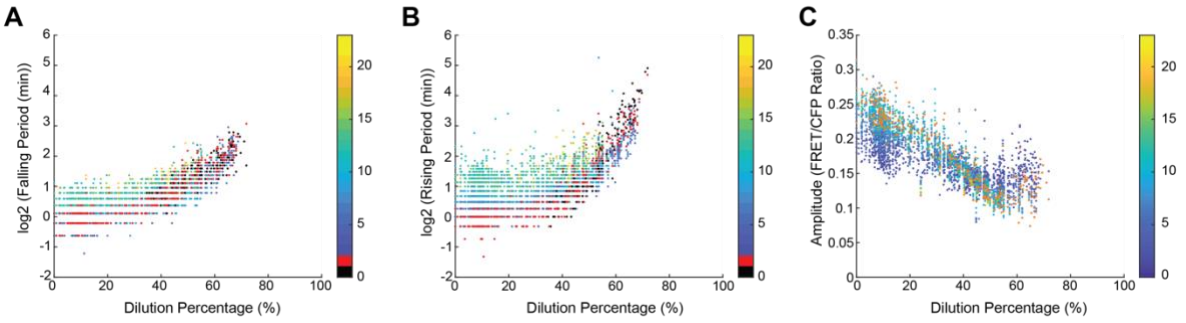

Figure S1: Dilution influences rising periods more pronouncedly than falling periods. (A) Fold changes of rising period (interphase) and (B) falling period (mitosis) for the extract in Fig 1. Dots in black are cycle 0 and dots in red are associated with cycle 1. Both interphase and mitosis are robust up to 40% dilution percentage (0.6x RCD), whereas rising periods have more significant fold changes (up to 4.8x) compared to falling periods (up to 2.9x) at high dilutions. Thus, interphase is more impacted than mitosis by dilution, manifesting the tighter regulations during mitosis. (C) the dynamic of amplitude as a function of dilution for the extract in Fig 1. Each dot represents one cycle. Amplitudes of the last cycle are usually disrupted and do not show an accurate measurement, so we label them in orange in the plot. Amplitudes first decrease as the system is being diluted, while near the oscillation threshold, amplitudes increase. This increase may be correlated to a significant period elongation in these droplets and the stoichiometry changes between Cdk1 and Cdk1-FRET sensor in highly diluted extracts.

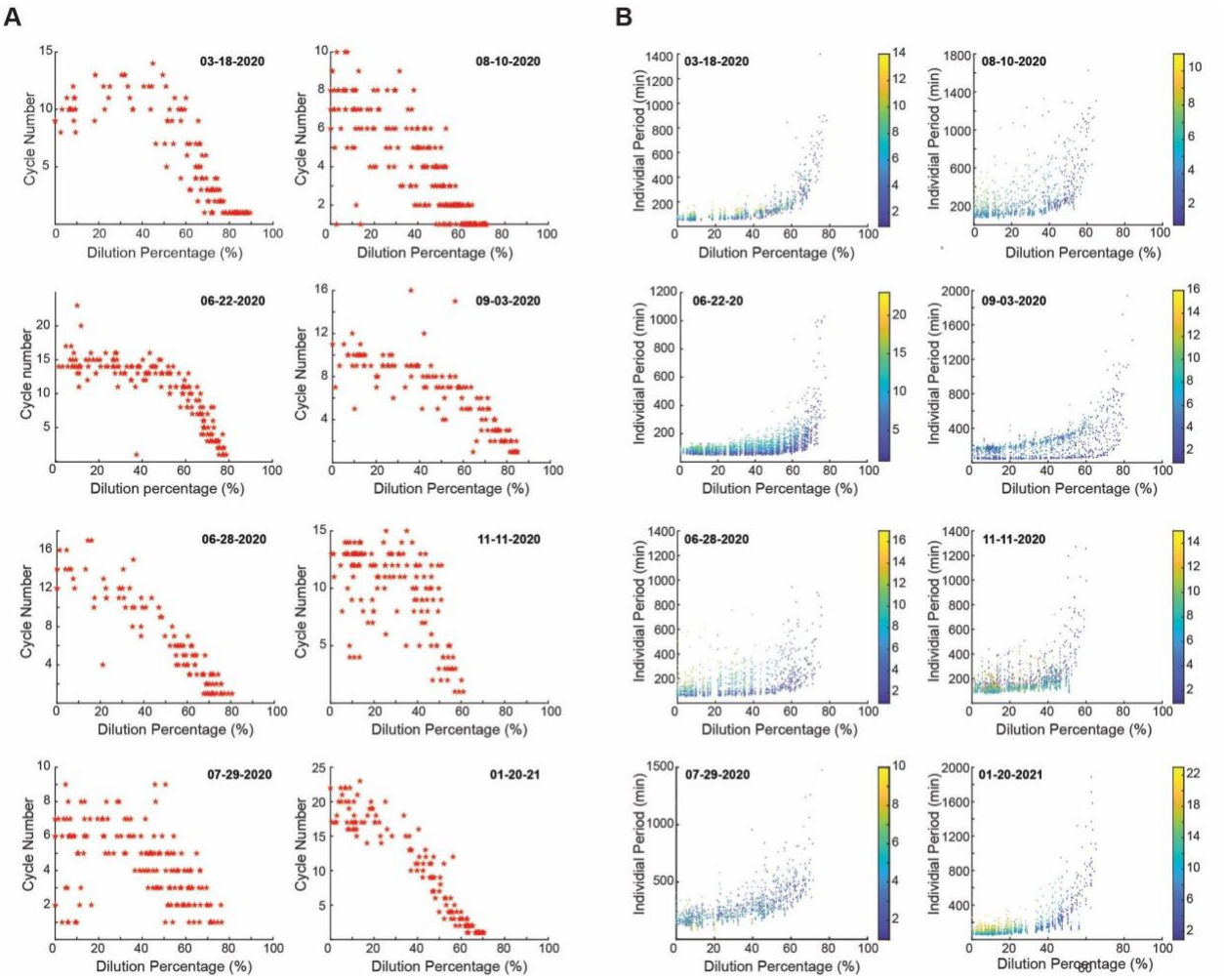

Figure S2: Even though there are some batch-to-batch variations, the overall trends of (A) cycle number and (B) period as a function of dilution are consistent across nine different day preparations (one is shown in Fig 1). Cycle numbers present a slight spike at moderate dilutions in two out of nine experiments; and in other three out of night experiments, cycle numbers decrease relatively linearly with dilutions. In the rest four experiments, cycle numbers show a plateau with low range of dilutions and then decrease abruptly at high dilution percentages. In most experiments, the period curve is relatively flat at the low dilution region and then has a drastic increase as the dilution percentage becomes high. Even though the absolute value of where periods start to significantly extend varies across these nine experiments, the overall trend is maintained.

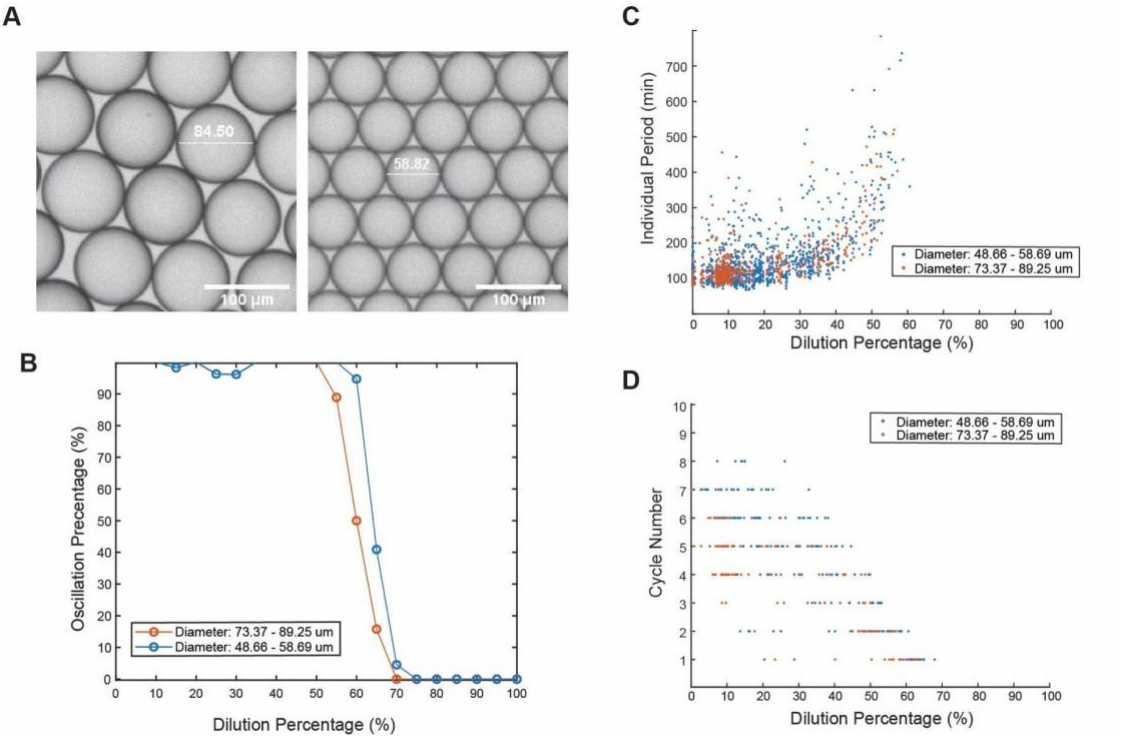

Figure S3: Partition errors are not associated with the halt of oscillation in highly diluted droplets. Droplets with (A) two different diameters: 83.18±2.21 µm and 55.29±1.83 µm show no significant difference in (B) oscillation percentage, (C) the total period, and (D) cycle number as a function of dilution percentage.

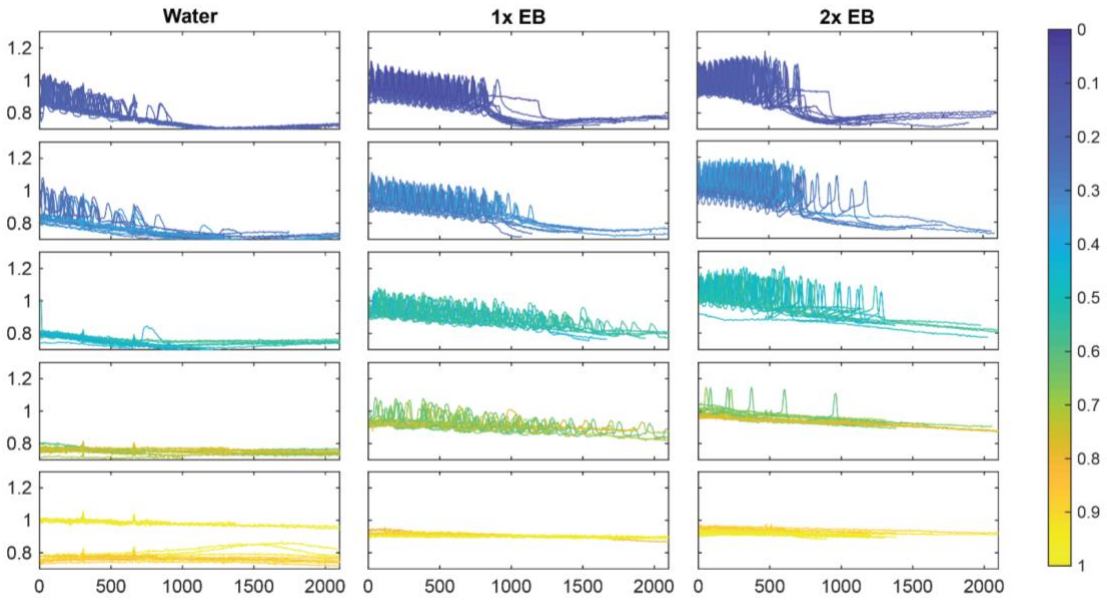

Figure S4: Dilution of cycling extracts with pure autoclaved deionized distilled water (ddH2O), 1x EB, and 2x EB. The system resists water dilution up to 40% before the oscillations arrest, whereas 1x EB and 2x EB show a comparable range of up to 70-80% dilutions before the system stops oscillations. Thus, the extract buffer (EB), with proper ionic strength or osmolarity, is essential for the system to function properly.

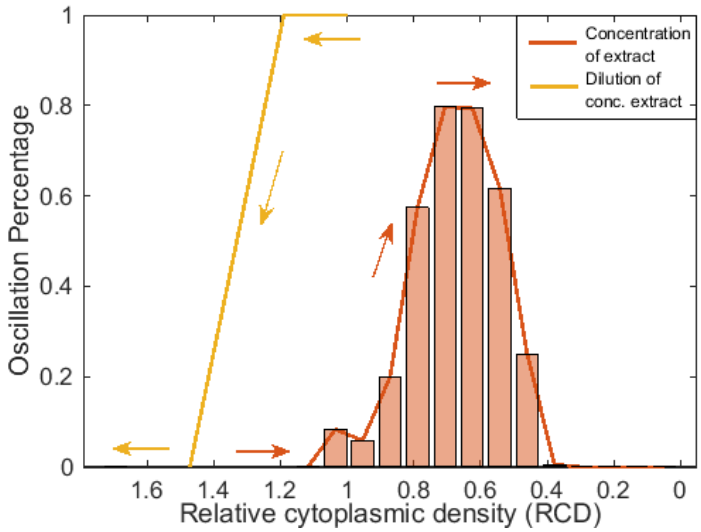

Figure S5: Hysteresis experiment using water for dilution. Experimental setup was the same as those in Fig 2 of the main text, except here we used autoclaved water rather than 1x EB for dilution. Hysteresis was observed when we concentrated extracts and diluted the non-oscillatory concentrated extracts back to oscillations.

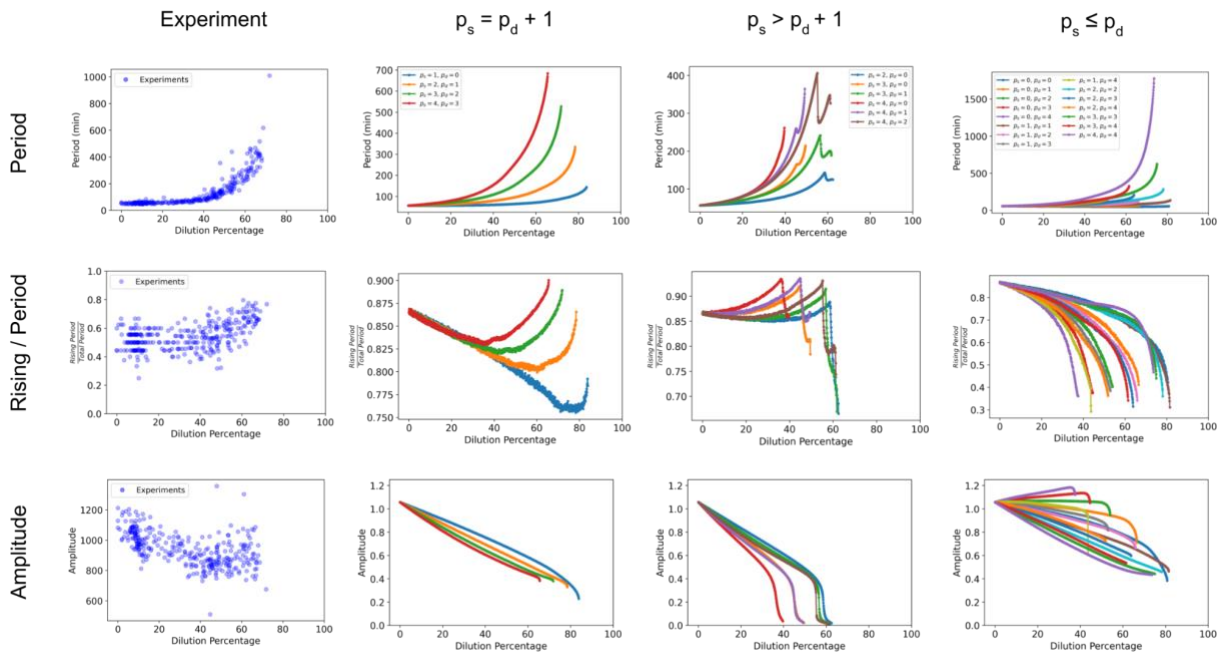

Figure S6: Selection of appropriate dependency of synthesis and degradation rate with cytoplasmic density. **Rows:** Three different quantities are analyzed from experiments and simulations as a function of dilution percentage. The total period, the fraction of the time the system spends in the rising phase, and the amplitude are used to compare experiments with simulations and choose the appropriate scaling for synthesis and degradation rate. **Columns:** Experiments and simulations. Simulations are separated into three groups according to the relationship between p_s and p_d and the behavior of the three quantities analyzed. All the possible integer combinations of ps and pd between 0 and 4 are studied.

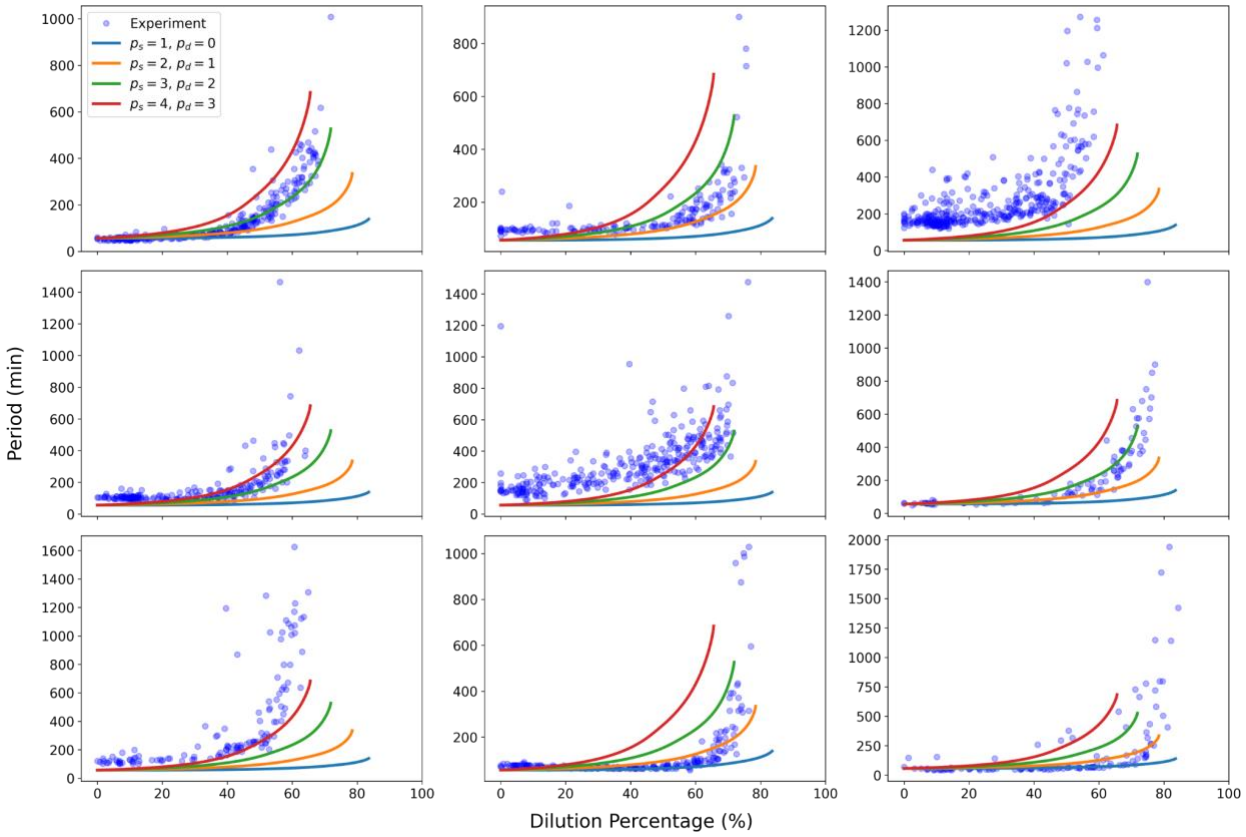

Figure S7: Comparison of selected models with experimental data. Each panel represents a different replicate for the experimental data. In all plots the four selected curves are presented. As a reference the leftmost top plot is the same dataset presented in Fig S6. The case $p_s = 3$, $p_d = 2$ (green curve) was used as a reference for further studies of the model.

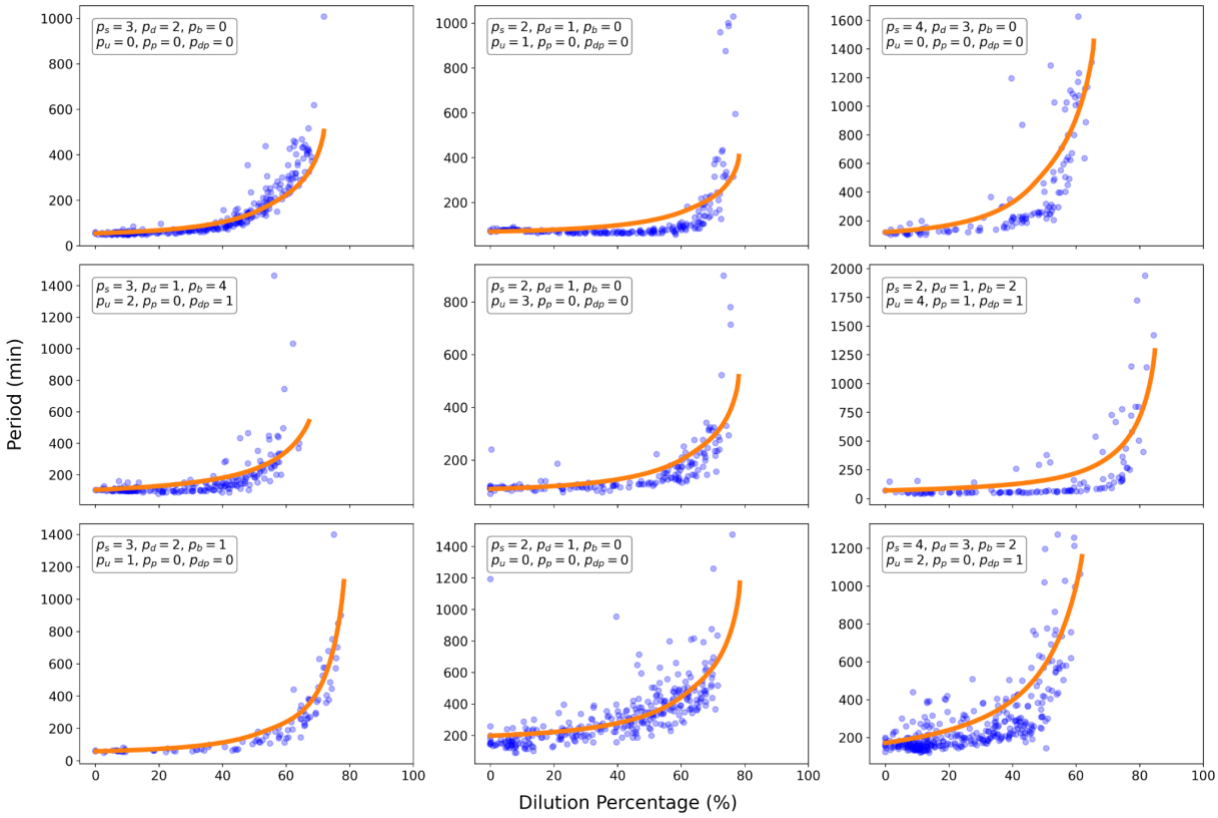

Figure S8: Comparison between experimental data (blue dots) and simulation (orange lines) for a model where binding/unbinding and phosphorylation/dephosphorylation rates can decay with dilution. Each panel corresponds to an experimental replica. The shown simulation curve is the one that best matches the data in terms of RMSD, behavior of the rising phase, and amplitude. Legend displays the parameters of the simulation.

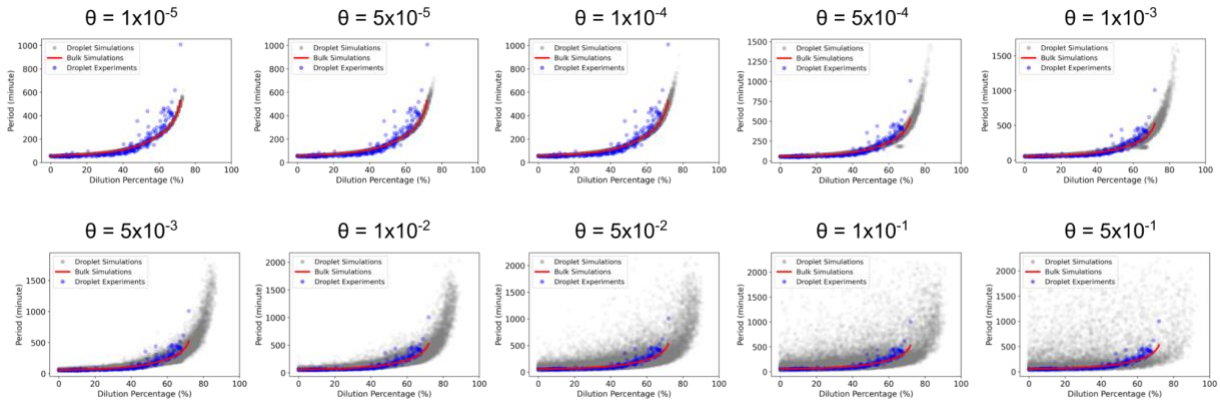

Figure S9: Droplet simulations with different variability in the parameter selection. Theta (θ) values were selected between 10^{-5} (droplets follow closely the bulk solution) and 10^{-1} (droplets deviate significantly from bulk solution). For the main text we selected a value of $\theta = 10^{-4}$ as it represented a level of variability similar to the experimental data as well as matched the observed coefficient of variation (CV) of fluorescent probe encapsulation.

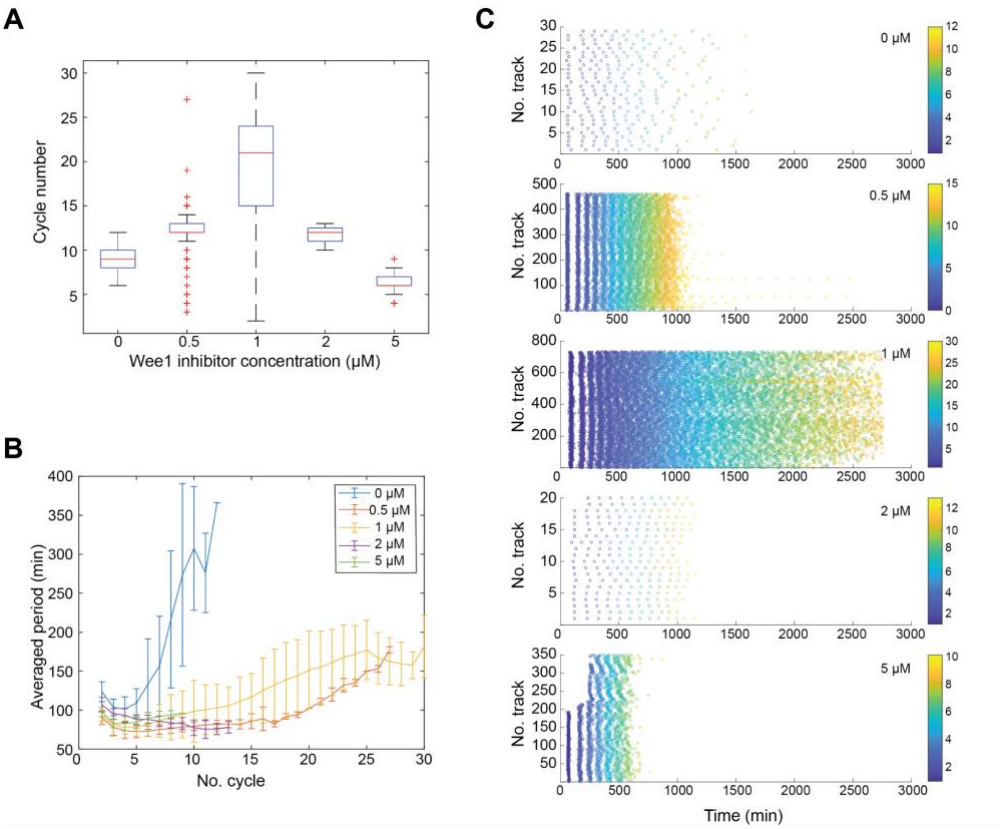

Figure S10: Wee1 inhibitor PD166285 modulates (A) cycle number, (B) the duration of periods, (C) the total oscillation time in extracts without dilutions. The duration of periods is shortened with wee1 inhibitor addition. The cycle number and total oscillation times of the extract respond to the inhibition of Wee1 non-monotonically: the system with 1μM Wee1 inhibitors shows the maximum cycle numbers and most prolonged total oscillation time.

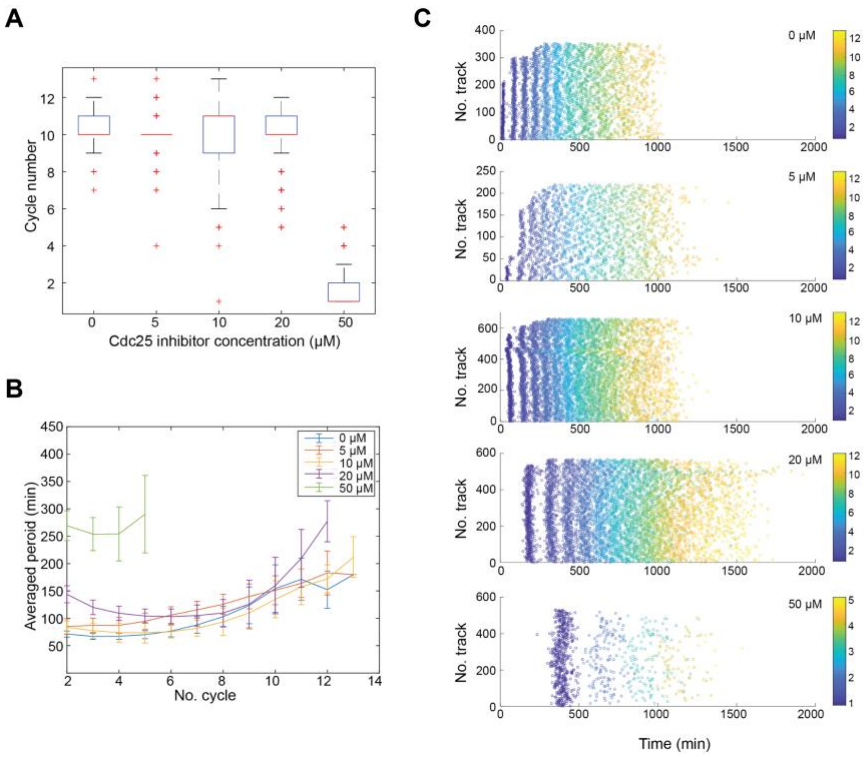

Figure S11: The influence of Cdc25 inhibitor NSC95397 on (A) cycle number, (B) the duration of periods, and (C) the total oscillation time in extracts without dilutions. System with Cdc25 inhibitor addition shows extended period length for early cycles, which is consistent with previous results reported in literature. Extracts with 50 μM inhibitors show less tendency to oscillate, so we assume this inhibition level is too high for maintaining normal oscillation behaviors. Besides the high 50 μM condition, the cycle number does not show a significant correlation with Cdc25 inhibition levels, but due to the prolonged period length, the total oscillation time is still extended as Cdc25 is being inhibited.

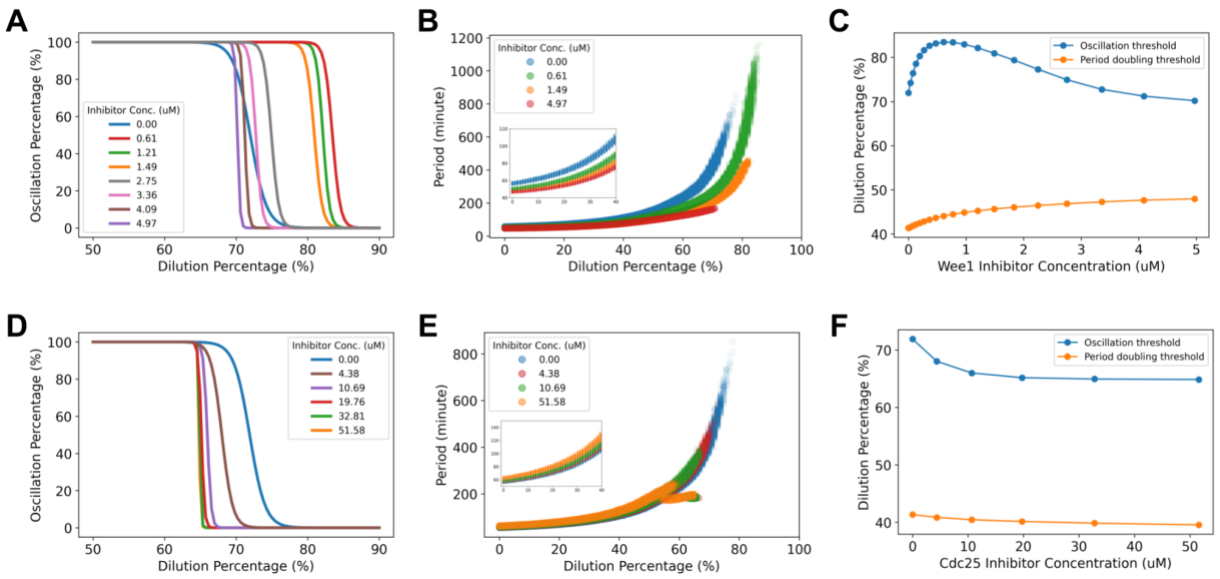

Figure S12: Simulation of the effect of Wee1 and Cdc25 inhibitors on robustness to dilution. For Wee1 inhibition different oscillation percentage curves are shown (A) as well as period (B) and thresholds (C). The same information is shown for Cdc25 inhibition in (D), (E), and (F). Oscillation thresholds are obtained from droplet simulations using the setup described in SI text S6. Period doubling thresholds are obtained from bulk simulations at each corresponding set of parameters. Insets in (B) and (E) show a zoomed version between dilutions 0% and 40%. In (A), (B), (D), and (E) only certain curves are shown for visual clarity.

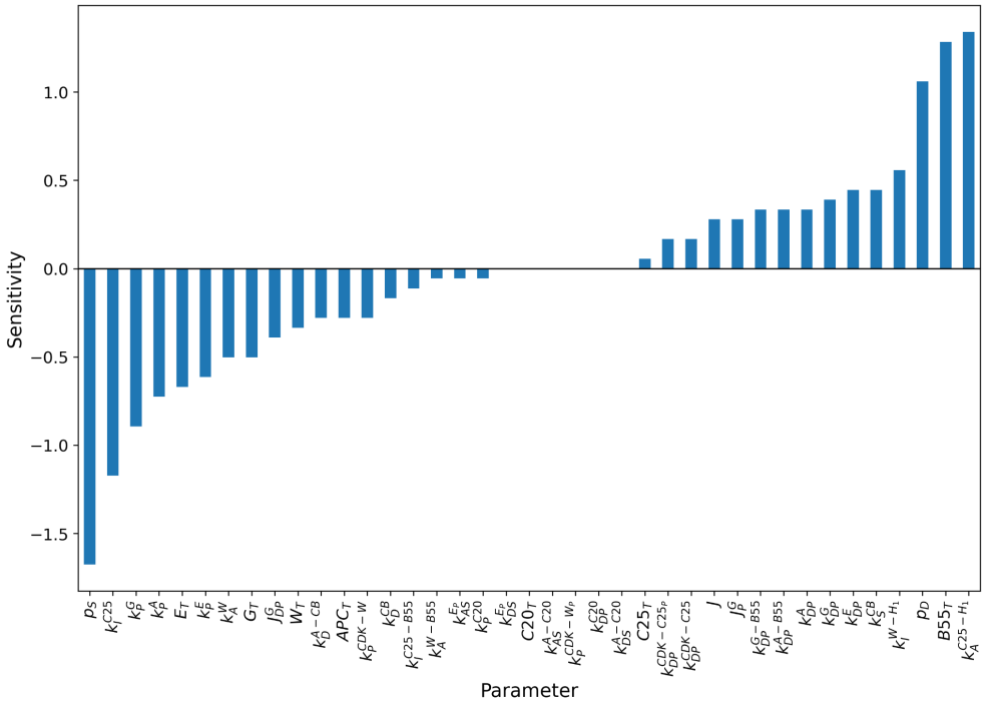

Figure S13: Parameter sensitivity analysis. Each parameter was increased by 1% and the percentage change in dilution threshold was calculated as the sensitivity. Positive sensitivity values indicate an increase in robustness while negative values indicate a decrease.

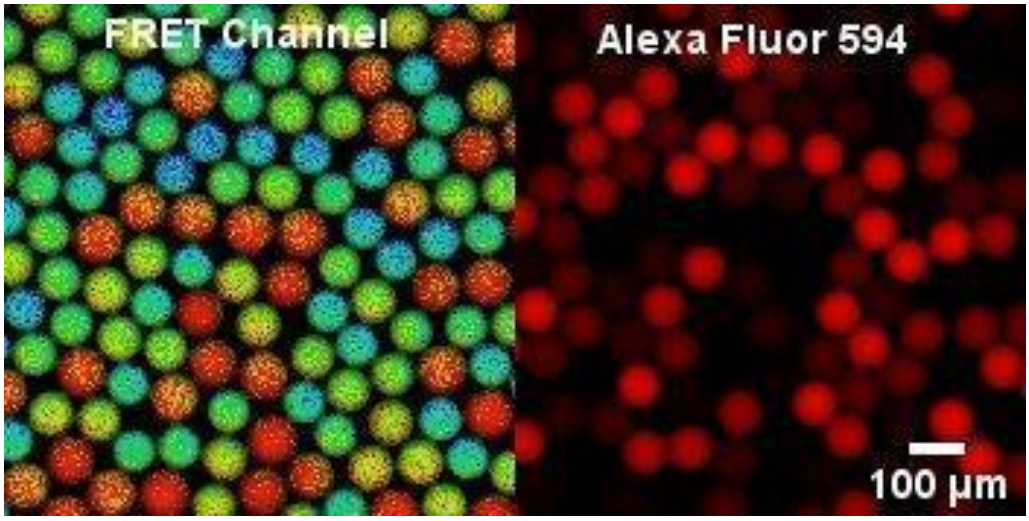

Snapshot of Movie S1: This video is corresponding to Fig 1B. The oscillation behaviors of droplets with different dilutions are recorded. A Cdk1-FRET sensor is added to indicate the Cdk1/PP2A activity in the extracts encapsulated in each droplet. In the FRET channel, droplets in red indicated high active Cdk1 levels as in mitosis, whereas cool blue color was associated with low active Cdk1 levels as in interphase. Droplets with intact mitotic oscillators were supposed to alternate from high to low Cdk1 states, resulting in droplets blinking over time. Alexa fluor 594 dextran dye is added as a dilution percentage indicator. Scale bar is 100 μm.

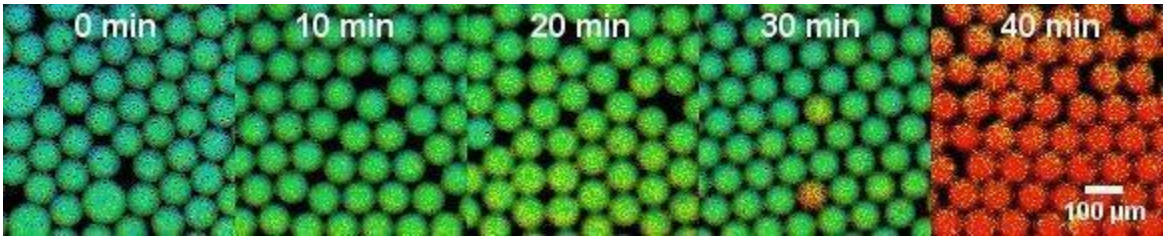

Snapshot of Movie S2: This is corresponding to the concentration experiment in Fig 2A-B. FRET channels for extracts concentrated with different evaporation time are presented. Extracts that are concentrated by vacuum evaporation for 0, 10, 20, 30 minutes still present intact oscillation behaviors, but the 40-min concentrated system stops oscillating.

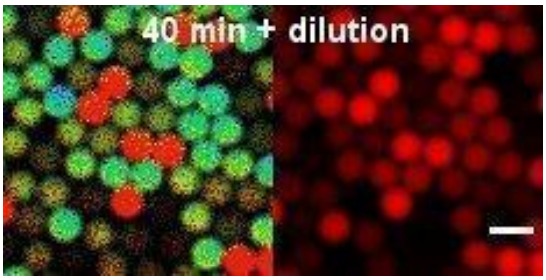

Snapshot of Movie S3: This is corresponding to the diluting of concentrated extract experiment in Fig 2B-I (Left: FRET channel for cell cycle monitoring; Right: Alexa fluor 594 channel for dilution percentage indication). Dilution of non-oscillatory 40-min concentrated extract restores oscillations. Scale bar is 100 μm.

SI text S1: Mathematical model and dependency of parameters with cytoplasmic density

We began our analysis using as reference a previously developed model of cell cycle dynamics (1). This model describes the regulation of Cdk1:CyclinB complex by Cdc25 and Wee1, the regulation of PP2A by GWL and ENSA, and the negative feedback loop composed of Cdc20 and APC/C. A diagram of the interactions between components is presented in the main text Fig 3A. To model the effect of a variable cytoplasmic density on the system's parameters we introduce a new parameter d, the relative cytoplasmic density. A value of $d = 1$ corresponds to the unperturbed cell cycle dynamics described by the equations of (1). The equations describing the dynamics of the system at different cytoplasmic densities are the following (newly introduced parameter d is shown in red for visual clarity):

- Cyclin B

$$\frac{d\mathrm{CB}}{dt} = d^{p_s} k_S^{CB} - d^{p_d}\left(k_D^{CB} + k_D^{A-CB}\frac{\mathrm{APC}_{C20}}{J+\mathrm{CB}}\right)\mathrm{CB}$$

- Cdk1:CycB complex

$$\begin{aligned}\frac{d\mathrm{CDK}}{dt} = &+ d^{p_s} k_S^{CB} - d^{p_d}\left(k_D^{CB} + k_D^{A-CB}\frac{\mathrm{APC}_{C20}}{J+\mathrm{CB}}\right)\mathrm{CDK} \\ &- \mathrm{vp}^{CDK}\mathrm{CDK} + \mathrm{vdp}^{CDK}(\mathrm{CB}-\mathrm{CDK})\end{aligned}$$

- Cdc25

$$\frac{d\mathrm{C25}_P}{dt} = k_A^{C25-H_1} H_1 \frac{C25}{J+C25} - (k_I^{C25} + k_I^{C25-B55} B55)\frac{C25_P}{J+C25_P}$$

- Wee1

$$\frac{d\mathrm{W}}{dt} = (k_A^W + k_A^{W-B55} B55)\frac{\mathrm{W}_P}{J+\mathrm{W}_P} - k_I^{W-H_1} H_1 \frac{W}{J+W}$$

- PP2A:B55δ complex

$$\frac{d\mathrm{B55}}{dt} = -k_{AS}^{E_P} * (E_P - B55_B)B55 + (k_{DS}^{E_P} + k_{DP}^{E})B55_B$$

- Ensa

$$\frac{d\mathrm{E}_P}{dt} = k_P^E G_P E - k_{DP}^E E_P$$

- Greatwall

$$\frac{d\mathrm{G}_P}{dt} = k_P^G H_1 \frac{G}{J_{DP}^G + G} - (k_{DP}^G + k_{DP}^{G-B55} B55)\frac{G_P}{J_P^G + G_P}$$

- Phosphorylation steps for APC partial activation

$$\begin{aligned}\frac{d\mathrm{APC}_{P1}}{dt} &= k_P^A H_1 \mathrm{APC} - (\mathrm{vdp}^A + k_P^A H_1)\mathrm{APC}_{P1} + \mathrm{vdp}^A \mathrm{APC}_{P2} \\ \frac{d\mathrm{APC}_{P2}}{dt} &= k_P^A H_1 \mathrm{APC}_{P1} - (\mathrm{vdp}^A + k_P^A H_1)\mathrm{APC}_{P2} + \mathrm{vdp}^A \mathrm{APC}_{P3} \\ \frac{d\mathrm{APC}_{P3}}{dt} &= k_P^A H_1 \mathrm{APC}_{P2} - (\mathrm{vdp}^A + k_P^A H_1)\mathrm{APC}_{P3} + \mathrm{vdp}^A \mathrm{APC}_{P4}\end{aligned}$$

$$\frac{d\mathrm{APC}_{P4}}{dt} = k_P^A H_1 \mathrm{APC}_{P3} - \mathrm{vdp}^A \mathrm{APC}_{P4}$$

- APC:Cdc20 complex

$$\begin{aligned}\frac{d\mathrm{APC}_{C20}}{dt} &= + k_{AS}^{A-C20}(\mathrm{APC}_{P4} - \mathrm{APC}_{C20})(\mathrm{C20} - \mathrm{APC}_{C20}) \\ &\quad - (k_{DS}^{A-C20} + \mathrm{vdp}^A + k_P^{C20} H_1)\mathrm{APC}_{C20}\end{aligned}$$

- Cdc20

$$\frac{d\mathrm{C20}}{dt} = k_{DP}^{C20} \mathrm{C20}_P - k_P^{C20} H_1 \mathrm{C20}$$

Auxiliary quantities

Cdk effective concentration for kinase activity
$\mathrm{H}_1 = \mathrm{CDK} + \alpha(\mathrm{CB} - \mathrm{CDK})$
Unphosphorylated Cdc25
$C25 = d \times C25_T - C25_P$
Phosphorylated Wee1
$W_P = d \times W_T - W$
CDK's phosphorylation rate
$\mathrm{vp}^{\mathrm{CDK}} = k_P^{\mathrm{CDK}-W} W + k_P^{\mathrm{CDK}-W_P} W_P$
CDK's dephosphorylation rate
$\mathrm{vdp}^{\mathrm{CDK}} = k_{DP}^{\mathrm{CDK}-C25_P} C25_P + k_{DP}^{\mathrm{CDK}-C25} C25$
B55δ bound to Ensa
$B55_B = d \times B55_T - B55$
Unphosphorylated Ensa
$E = d \times E_T - E_P$
Unphosphorylated Greatwall
$G = d \times G_T - G_P$
Unphosphorylated APC
$\mathrm{APC} = d \times \mathrm{APC}_T - \mathrm{ACP}_{P1} - \mathrm{ACP}_{P2} - \mathrm{ACP}_{P3} - \mathrm{ACP}_{P4}$
APC's dephosphorylation rate
$\mathrm{vdp}^A = k_{DP}^{A-B55} B55 + k_{DP}^A$
Phosphorylated Cdc20
$C20_P = d \times C20_T - C20$

Where we explicitly model the effect of cytoplasmic density on the system's parameters. First, we assumed that reaction rates of association/dissociation and phosphorylation/dephosphorylation do not depend on cytoplasmic density. Our reasoning is that changes in these microscopic rates will be less important than the changes due to variations in the total concentration of reactants. We realize that changes in viscosity and the properties of the medium can affect these microscopic rates but we chose not to consider those in our first approximation to the phenomenon. Similarly, we assume that Michaelis constants do not vary with cytoplasmic density since in turn these are described by microscopic rates. Second, we assumed that total concentrations scale linearly with cytoplasmic density because experimentally only buffer is added to/removed from the system and not cell cycle's components. Finally, we considered the effect of changes in cytoplasmic density on synthesis and degradation rate of cyclin B. These rates are expected to be affected by dilution and concentration of the system. Each reaction is composed of multiple intermediary steps which are not explicitly described in the proposed model. Both processes are described effectively with synthesis having a constant production rate and degradation as a first-order reaction. We maintained these simplified descriptions of both processes and explored different hypotheses for possible dependencies with cytoplasmic density. Our guide was the observed changes in cell cycle dynamics due to dilution and concentration. We assumed that synthesis and degradation are scaled by a power of the

relative cytoplasmic density denoted p_s and p_d respectively. Both are undetermined parameters and in SI text S2 we discuss our methodology for the selection of their values.

SI text S2: Parameter values

The parameters used in our article for the description of physiological cycles slightly differ from those in (1). Specifically, we employed a different synthesis rate since bifurcation diagrams with this higher value of the parameter agreed better with experimental observations. Additionally, the timescale of the system was redefined to match the average observed physiological period in experiments. The timescale was redefined by scaling all reaction rates by a factor of 0.5. The reference physiological parameters used in this study are presented in Table S2.

Total concentrations

APC_T	1.5	E_T	2.2
$\mathrm{C25}_T$	1.0	G_T	1.0
W_T	1.0	$\mathrm{B55}_T$	0.7
$\mathrm{C20}_T$	2.0		

Synthesis and degradation

k_S^{CB}	0.05	k_D^{A-CB}	1.0
k_D^{CB}	0.01		

Phosphorylation and Dephosphorylation

k_A^W	0.1	k_P^{C20}	2.0
k_A^{W-B55}	0.15	k_{DP}^{C20}	1.0
$k_A^{C25-H_1}$	0.5	$k_I^{W-H_1}$	0.5
k_{DP}^A	0.05	k_I^{C25}	0.1
k_{DP}^{A-B55}	0.75	$k_I^{C25-B55}$	0.15
k_{DP}^E	1.0	k_P^A	0.25
k_{DP}^G	0.05	k_P^E	2.0
k_{DP}^{G-B55}	0.5	k_P^G	0.5
$k_{DP}^{CDK-C25}$	0.1	k_P^{CDK-W}	2
$k_{DP}^{CDK-C25_P}$	1.0	$k_P^{CDK-W_P}$	0.01

Association and Dissociation

k_{AS}^{A-C20}	250	$k_{AS}^{E_P}$	250
k_{DS}^{A-C20}	0.5	$k_{DS}^{E_P}$	0.5

Miscellaneous

α	0.3	J_P^G	0.1

J	0.01	J_{DP}^{G}	

Table S2: Parameters of the mathematical model describing cell cycle oscillations.

Where we keep the same convention as in (1) of concentrations being in arbitrary units and time being represented in minutes. We have two undetermined parameters in our model, p_S and p_D. They represent the changes in synthesis and degradation rate as the cytoplasmic density is modified. As an example, if protein synthesis was simply described as a second-order reaction between total mRNA and ribosomes, we would expect $p_S = 2$ to account for the decay of both total concentrations. Similarly, if degradation was effectively a reaction between the proteasome and the substrate, we would expect $p_D = 1$ to account for the scaling of proteasome concentration. However, given that both synthesis and degradation are mediated by multiple intermediaries, we decided to explore different values of p_s and p_d. We considered all possible integer combinations between 0 and 4 for both parameters. For each combination we compared experiments and simulations in terms of the period of the oscillations, the amount of time spent in the rising phase and the amplitude. Using these three features we filtered out those parameter combinations that did not follow experimental trends.

We considered specific experimental observations to select the most appropriate model. First, we expect the period to increase as a function of dilution and oscillations to stop in a range between 60% to 80%. Second, close to the threshold rising periods become elongated, which translates to an increase in the fraction of rising period to total period. Third, amplitude should decay with dilution and display a finite value at the threshold in contrast to decaying continuously to zero. We simulated and measured these quantities for all studied combinations of p_s and p_d. The results can be appreciated in Fig S6. Simulation details are described in SI text S6.

We observed that simulation results could be clustered into three groups. While most simulations show a period that increases with dilution, the behavior for the rising fraction and amplitude is different between simulations with $p_s = p_d + 1$, $p_s > p_d + 1$, and $p_s \leq p_d + 1$. The only group that meets the three conditions observed in the data is the one where $p_s = p_d + 1$. Namely, period increases with dilution, thresholds are between 60% and 80%, rising fraction increases just before oscillations stop, and amplitude decreases without dropping to 0 near the threshold. In contrast, the other groups show features not observed in data. The group $p_s > p_d + 1$ presents an amplitude that decays continuously to zero with sudden jumps in period near the threshold. The group $p_s \leq p_d + 1$ displays a decreasing rising fraction as a function of dilution in disagreement with experimental observations. Therefore, we selected the models with $p_s = p_d + 1$ for further analysis

We compared the selected simulation curves ($p_s = p_d + 1$) with different experimental replicates (Fig S7). A great variability in the response to dilution is observed in experiments regarding the exact period of the oscillations. However, all curves displayed the same trend: increase in period with a sudden stop of oscillations consistent with our selected models. We arbitrarily selected the case $p_s = 3$, $p_d = 2$ to present in the main text but other specific values of p_s and p_d that satisfy $p_s = p_d + 1$ agree with specific experimental days equally well. Given our level of description, p_s and p_d represent the modulation of those processes driving the increase and decrease of active cyclin B1:Cdk1 rather than cyclin's synthesis and degradation rate. The increase of kinase complex is associated with cyclin B1 mRNA translation, Cdk1's binding to cyclin B1, and complex activation via CAK and Cdc25. On the other hand, the decrease in the mitotic complex is driven by Cdk1's unbinding from cyclin, cyclin ubiquitination via APC, proteasome-mediated degradation, and inactivation via Wee1. Therefore, our modeling suggests that some of these processes need to be affected by dilution for the model to describe the observed trend in the period.

We also analyzed whether binding/unbinding and phosphorylation/dephosphorylation rates decay with dilution. It is possible for these processes to vary due to changes in crowding, diffusion, or viscosity as the system is diluted. Apart from p_s and p_d we included four additional undetermined parameters: p_b, p_u, p_p, and p_{dp} for the aforementioned reactions. Note that the same decay applies to every reaction in the same category. We simulated all integer combinations between 0 and 4 of these six parameters and then

compared experimental results with their simulated counterparts. The comparison was performed using both the root mean square deviation of the period (RMSD)

$$RMSD = \sqrt{\frac{\sum_{i=1}^{N}(P_{exp}^{i} - P_{sim}^{i})^2}{N}}$$

and two key experimental features (as in Fig S8): the rising phase has to increase more than the falling phase, and amplitude has a finite value at the threshold. Fig S8 shows the period curve for the best four matches for each experimental day. It can be appreciated that each experimental day has different values for the decay parameters. In particular, some experimental days have non-zero values for the decay of binding/unbinding and phosphorylation/dephosphorylation. These results suggest that the causes of dilution can also be attributed to a decay in the reaction rates between cell cycle components other than synthesis and degradation rate.

SI text S3: Encapsulation error and droplet simulations

Next, we explored the possibility of droplet-to-droplet variability due to encapsulation effects. It has previously been shown that encapsulation can modify the behavior of oscillators (2). Here we will adopt the same mathematical framework to describe this effect by using a gamma distribution to draw certain parameters in our model and generate a population of *in silico* droplets. We consider total concentrations as well as synthesis and degradation rate to be affected by this unequal partitioning. On the other hand, we do not consider microscopic reaction rates to be affected by this partition. Here, we retain the same working hypothesis that the major changes in reaction rates come from variations in the total concentration of reactants.

The probability density we adopt for sampling our parameters takes the form

$$p(x) = \frac{x^{k-1}}{\theta^k \Gamma(k)} e^{-x/\theta}$$

Where x is the parameter being sampled, k the shape of the distribution, θ its scale, and $\mathbf{\Gamma}$ the gamma function. The gamma distribution allows us to set the mean and variance independently. Given that the mean value of x under this distribution is given by kθ we assign

$$k = \frac{\mathrm{Param}_{\mathrm{Ref}}}{\theta}$$

To center the distribution around the corresponding bulk reference parameter. Then, θ becomes a free parameter that describes the variability of the parameter being sampled. From experiments we can estimate the coefficient of variation (std/mean) when encapsulating a fluorescent probe. Estimates taken from experiments in Table S1, produce a CV in the order of 1e-2. Since the standard deviation of the selected distribution is $k\theta^2$, with our choice of k we have

$$CV = \sqrt{\frac{\theta}{\mathrm{Param}_{\mathrm{Ref}}}}$$

Since model parameters are in relative units, we plug in a value of $\mathrm{Param}_{\mathrm{Ref}} = 1$ for estimating θ. With a CV of 1e-2, we estimate θ to be

$$\theta \approx 10^{-4}$$

Therefore, to simulate individual droplets, we draw total concentrations, synthesis rate, and degradation rates from a gamma distribution centered on our selected reference parameters (Table S2). For completion, we simulated the system under different values of θ (Fig S9). When compared with the variability and

characteristics of the experimental data, a value of θ = 1e-4 seems appropriate to describe the variability between droplets: larger values present a variability not seen in experiments and smaller values follow too closely the bulk solution.

SI text S4: Wee1 and Cdc25 Inhibitors

To simulate the effect of inhibitors, we introduce additional parameters in the system. The reaction rate of Wee1 and Cdc25 activity on Cdk1 is multiplied by new variables I_W and I_C respectively. The modified equation for Cdk1 reads:

$$\frac{d\mathrm{CDK}}{dt} = + d^{p_s} k_S^{CB} - d^{p_d} \left(k_D^{CB} + k_D^{A-CB} \frac{\mathrm{APC}_{C20}}{J + \mathrm{CB}} \right) \mathrm{CDK} - I_W \mathrm{vp}^{CDK} \mathrm{CDK} + I_C \mathrm{vdp}^{CDK} (\mathrm{CB} - \mathrm{CDK})$$

Where a value of I_W and I_C of 1 represents the system without inhibitors added. By simulating the system for values between 0 and 1 of the new parameters we can mimic the effect of inhibitors that reduce the activity of Wee1 and Cdc25 on Cdk1.
To connect simulation results with experiments we assume a Hill effect of the inhibitors on the enzyme's activity. Therefore, the inhibition parameters are connected to the concentration of inhibitor via

$$I_W \quad \text{or} \quad I_C = \frac{1}{1 + C/K_I}$$

Where C represents the inhibitor concentration and K_I the unknown inhibition constant. For Wee1 inhibition and Cdc25 inhibition we simulate a population of droplets for both dilutions (d) and inhibitions (I_W or I_C) between 0 and 1. We process our results to obtain the oscillation percentage, period, and thresholds at each inhibition percentage (Fig S12). Results are converted to inhibitor concentration by exploring different values of K_I and selecting the value that resembles experimental observations more closely. For Wee1 simulations we used a value of K_I = 0.175 uM. For Cdc25 simulations we used K_I = 10 uM.

SI text S5: Sensitivity analysis

The mathematical model employed in this manuscript has several parameters describing the processes driving cell cycle oscillations. Here, we explore which parameters when changed affect the most the robustness to dilution. We increased each parameter of the model by 1% and measured the dilution at which oscillations disappeared (Threshold 1%). Then we compared that dilution to the reference value when the parameter was not changed (Threshold Ref). This allowed us to calculate the sensitivity as

$$\mathrm{Sensitivity} = \frac{\mathrm{Threshold\ 1\%} - \mathrm{Threshold\ Ref}}{\mathrm{Threshold\ Ref}}$$

The result is presented in Fig S13. This analysis suggests the most interesting parameters to vary in future experiments. The decay of both synthesis and degradation (p_s and p_D) appear as great contributing factors. Similarly the activation of Cdc25 and Greatwall by Cdk1 appears as important variables when determining the robustness to dilution. Finally, the total concentration of PP2A could be explored to change the system's robustness. As confirmed by experiments and simulations the activity of Wee1 and Cdc25 towards Cdk1 is not a parameter of the model that when changed greatly affects the robustness to dilution.

SI text S6: Simulation details and analysis

All time series are obtained by numerical integration of the ODE equations. Simulations were performed in Python 3.7.10 using the function solve_ivp from the package scipy 1.4.1. The selected integration method was LSODA. Oscillatory or steady-state behavior is determined by the norm of the system's velocity-vector in conjunction with an analysis of the signal's peak detection features. Namely, the period stability (variability in time differences between detected peaks) and amplitude stability (variability in peak concentrations) are analyzed. Peaks were detected with the function find_peaks from the same scipy package version. Droplet simulations are ODE simulations where the corresponding total concentrations, synthesis rate, and degradation rate are sampled from a Gamma distribution representing the encapsulation error. In all cases, 500 droplets are simulated per relative cytoplasmic density value. For various utilities numpy 1.19.4, pandas 1.2.1, and matplotlib 3.3.3 are used. Bifurcation diagram in 3I is performed in XPPAUT 8.0. The diagram starts from a high dilution converged steady state. Stable and unstable steady states are first tracked while the Hopf bifurcations are continued in a second iteration of the algorithm. AUTO parameters used for the scanning are: Ntst = 60, Ds = 0.01, Dsmin = 0.001, Dsmax = 0.1, ParMin = 0, ParMax = 2.5. The remaining parameters are set to their default values. In all cases except for the blue curve in 3J, all simulations started from the same initial condition as in (1) rescaled by the appropriate dilution. The blue curve in 3J uses as the initial condition the steady state of the system when the relative cytoplasmic density is 2.5.

Supplemental References

1. T. Zhang, J. J. Tyson, B. Novák, Role for regulated phosphatase activity in generating mitotic oscillations in Xenopus cell-free extracts. *Proc. Natl. Acad. Sci. U. S. A.* **110**, 20539-20544 (2013).
2. M. Weitz, J. Kim, K. Kapsner, E. Winfree, E. Franco, F. C. Simmel, Diversity in the dynamical behaviour of a compartmentalized programmable biochemical oscillator. *Nat. Chem.* **6**, 295–302 (2014).